


JULGI-mediated increment in phloem transport capacity relates to fruit yield in tomato

Hoyoung Nam¹ , Aarti Gupta¹, Heejae Nam¹, Seungchul Lee¹ , Hyun Seob Cho¹, Chanyoung Park¹, Soyoung Park¹, Soon Ju Park² and Ildoo Hwang^{1,*}

¹Department of Life Sciences, POSTECH Biotech Center, Pohang University of Science and Technology, Pohang, Korea

²Division of Biological Sciences and Research Institute for Basic Science, Wonkwang University, Iksan, Korea

Received 28 July 2021;

revised 19 April 2022;

accepted 21 April 2022.

*Correspondence (Tel +82-054-279-2291;

fax +82-054-279-0629; email

ihwang@postech.ac.kr)

Summary

The continuous growth of the global population and the increase in the amount of arid land has severely constrained agricultural crop production. To solve this problem, many researchers have attempted to increase productivity through the efficient distribution of energy; however, the direct relationship between the plant vasculature, specifically phloem development, and crop yield is not well established. Here, we demonstrate that an optimum increase in phloem-transportation capacity by reducing *SIJUL* expression leads to improved sink strength in tomato (*Solanum lycopersicum* L.). *SIJUL*, a negative regulator of phloem development, suppresses the translation of a positive regulator of phloem development, *SISMXL5*. The suppression of *SIJUL* increases the number of phloem cells and sucrose transport, but only an optimal reduction of *SIJUL* function greatly enhances sink strength in tomato, improving fruit setting, and yield contents by 37% and 60%, respectively. We show that the increment in phloem cell number confers spare transport capacity. Our results suggest that the control of phloem-transport capacity within the threshold could enhance the commitment of photosynthates to instigate yield improvement.

Keywords: CRISPR-Cas9, phloem development, plant productivity, *SMXL5*, source-sink partitioning, virus-induced gene silencing.

Introduction

Dietary shifts and the growing human population, along with the limited availability of arable land, pose enormous challenges to agriculture (Ehrlich and Harte, 2015; Ray *et al.*, 2013; Taiz, 2013). In addition, climate change and the associated increase in the frequency of extreme heat, drought, and flooding around the globe further reduce yield potential (Mills *et al.*, 2018).

To ensure a progressive increase in food production, various strategies have been proposed to engineer traits related to crop yields (Bailey-serres *et al.*, 2019; Long *et al.*, 2015); for example, controlling plant architecture by modulating the gibberellin or cytokinin phytohormone pathways could dramatically enhance wheat (*Triticum aestivum* L.) and rice (*Oryza sativa* L.) yields (Ashikari *et al.*, 2005; Peng *et al.*, 1999; Sasaki *et al.*, 2002). Another important strategy is to achieve a crop with highly efficient photosynthesis, as proposed by Price *et al.*, with the potential addition of genetic components from cyanobacteria into the plant to increase CO₂ uptake and improve yield traits (Price *et al.*, 2008). Photoassimilate loading and partitioning have also been targeted to improve crop yields (Lu *et al.*, 2020; Regmi *et al.*, 2020; Smith *et al.*, 2018; Weichert *et al.*, 2017; Yadav *et al.*, 2015; Zhang *et al.*, 2015; Zhu *et al.*, 2021). However, due to the limited amount of resources generated in photosynthesis and the complexity of the signalling networks, which encompass nutrients, phytohormones, and environmental factors, there is a limit to engineering carbon and nitrogen partitioning within plants (Yu *et al.*, 2015). Likewise, increasing the rate of photoassimilate loading into the sink organs often puts a strain on the source organ, negatively affecting the growth of plants (Dasgupta *et al.*, 2014). The potential for increasing plant productivity through the optimized distribution of photoassimilates to the

yield-associated organs has thus been an important focus of recent research (Osorio *et al.*, 2014; Ruan *et al.*, 2012; White *et al.*, 2016; Yadav *et al.*, 2015).

Land plants have evolved unique vascular system in which phloem tissues facilitate the long-distance transport of photosynthates, growth regulators, and inorganic nutrients (Cho *et al.*, 2017; Heo *et al.*, 2014; López-Salmerón *et al.*, 2019; Zhang and Turgeon, 2018), playing a critical role in the distribution of energy from the source to the sink organs. The *PHLOEM PROTEIN 2* promoter (*PP2*)-driven transgenic expression of *Arabidopsis thaliana* *SUCROSE TRANSPORTER 2* (*AtSUC2*) in rice enhanced its sucrose transport and increased yields without penalizing plant growth (Wang *et al.*, 2015). However, the transport phloem often exhibits a spare transport capacity where the sink exerts regulation on the flow capacity (Lucas *et al.*, 2013; Patrick, 2013). Driving the energy distribution towards sink tissues is likely a critical step for improving crop yield; however, it is unclear how the phloem cell count correlates to biomass production in plants.

In this study, we identified an orthologue of *Arabidopsis thaliana* *JULGI 1* (*AtJUL1*), a negative regulator of phloem development (Cho *et al.*, 2018), in tomato (*Solanum lycopersicum* L.). Here, we provide *in planta* evidence to demonstrate that *SIJUL* suppresses *SISMXL5* expression to regulate phloem development and fruit yield. The *SIJUL* knockdown did not cause growth retardation, but enhanced phloem development and transport capacity, leading to a significantly increased fruit set and sugar content in tomato. On the contrary, a complete loss-of-function in *SIJUL* resulted in the prolific phloem tissue and severe growth retardation which most likely is responsible for the compromised plant yield. Our results demonstrate that the distribution of photoassimilates through the phloem could shape yield potential in tomato and other crop plants.

Results

JUL1 function is conserved in tomato and predominantly expressed in its vascular tissues

To explore phloem development in tomato, we first searched for an orthologue of AtJUL1, a negative regulator of phloem development (Cho *et al.*, 2018). We identified a gene, *Soly-c08g067180.3.1* (*SIJUL*), encoding a protein sharing 116/178 (65%) of the same amino acids as the *Arabidopsis* orthologue and three RanBP2-type Zinc finger (ZnF) domains. Each domain contains a conserved arginine residue (R20, R81, and R151 in ZnF1, ZnF2, and ZnF3, respectively) (Figure 1a), which is required for RNA binding (Cho *et al.*, 2018; Nguyen *et al.*, 2011). Previously, our group demonstrated that AtJUL1 binds to the G-quadruplex in the 5' UTR region of *SUPPRESSOR OF MAX2 1-LIKE 5* (*AtSMXL5*), preventing the incorporation of *AtSMXL5* transcripts into translationally active ribosomes and thus preventing the biosynthesis of *AtSMXL5* protein (Cho *et al.*, 2018). *Soly-c07g018070.3.1* (*SISMXL5*) was identified as an orthologue of *AtSMXL5* (Cho *et al.*, 2018).

Using a computational scoring algorithm that predicts the G-score based on the number of G-tetrads and the length of loops connecting the G-tetrads (Kikin *et al.*, 2006), we predict that the 5' UTR of *SISMXL5* may also form a G-quadruplex (G-quadruplex in *AtSMXL5* 5' UTR has a score of 41, while for the *SISMXL5* 5' UTR the score is 39). We also found that *SIJUL* is located in both the cytoplasm and the nucleus (Figure S1), which corroborates with its previously established function in RNA binding and the subsequent restriction of the target transcripts into translationally active ribosomes. Therefore, we tested whether, similar to the AtJUL-*AtSMXL5* regulatory module (Cho *et al.*, 2018), the binding of *SIJUL* to the 5' UTR G-quadruplex of *SISMXL5* affects its translation. The protoplasts were co-transfected with a reporter *SISMXL5* 5' UTR fused upstream to the *GFP* gene and with *SIJUL* as an effector. The GFP signal was reduced by the addition of the *SIJUL* effector in a dose-dependent manner, but there was no change in the level of *GFP* mRNA. To demonstrate the RNA-binding activity of *SIJUL* to its target *SISMXL5*, we mutated the conserved arginine(s) to alanine(s) in *SIJUL* to create *SIJUL*^{R20/R81/R151A}. Protoplasts co-transfected with *SIJUL*^{R20/R81/R151A} and *SISMXL5* 5' UTR-fused *GFP* had GFP signals similar to those transfected only with *SISMXL5* 5' UTR-fused *GFP* (Figure 1b).

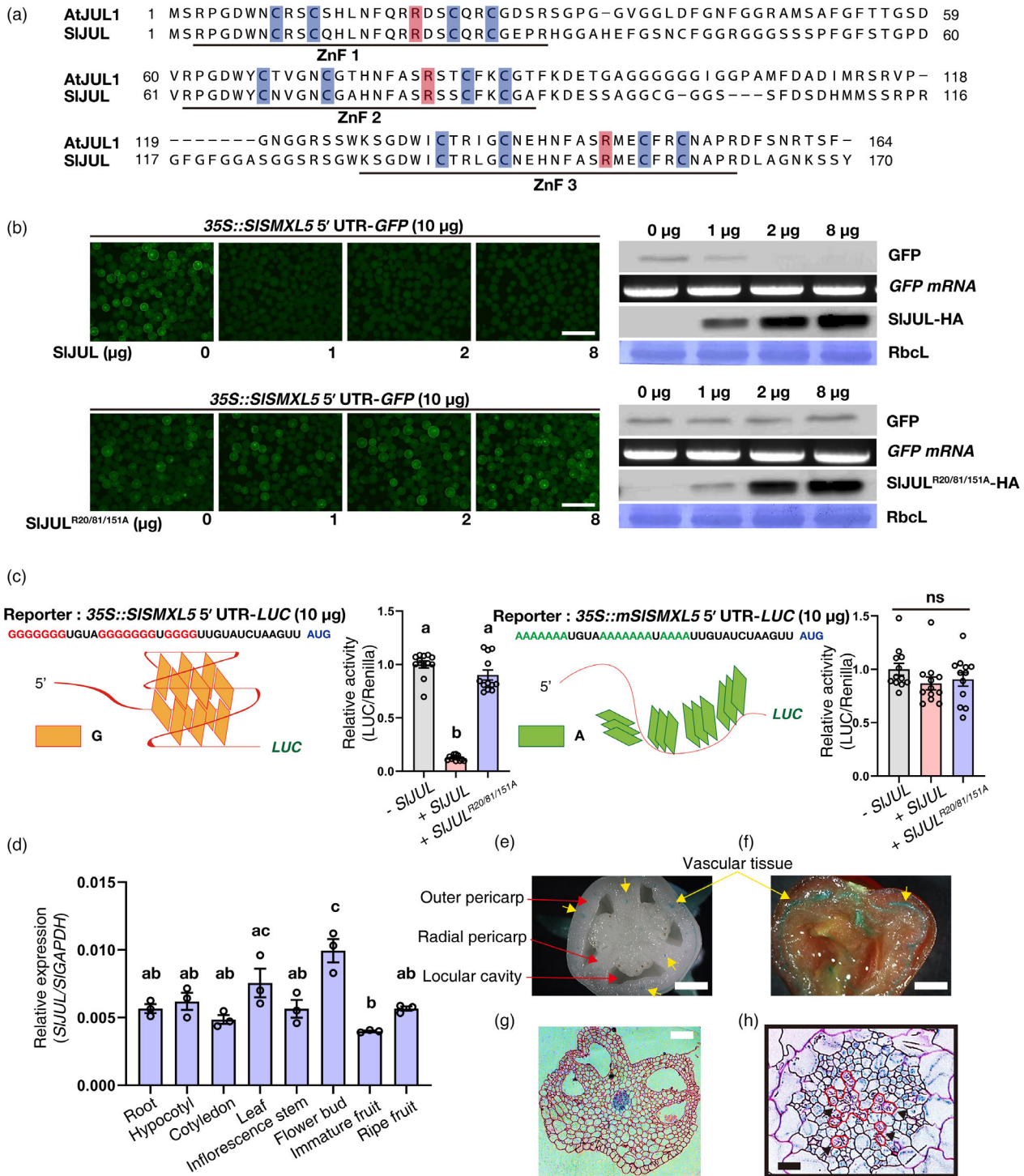
Consistent with these results, the protoplasts transfected with the *SISMXL5* 5' UTR-fused *luciferase* (*LUC*) reporter also showed a *SIJUL*-dependent decrease, whereas the mutations disrupting G-quadruplex formation in the *SISMXL5* 5' UTR (*mSISMXL5* 5' UTR) or the mutated *SIJUL*^{R20/R81/R151A} effector failed to suppress the target translation (Figure 1c). These data suggest that the interaction of *SIJUL* with the RNA G-quadruplex motif and the presence of an intact G-quadruplex in the *SISMXL5* 5' UTR are indispensable for the *SIJUL*-dependent suppression of *SISMXL5* translation.

To gain further insight into the function of *SIJUL*, we evaluated the spatial pattern of *SIJUL* expression in different organs spanning the early to late developmental stages. The expression profiles, determined using quantitative RT-PCR, revealed the ubiquitous presence of *SIJUL* transcripts in the root, hypocotyl, cotyledons, leaf, stem, flower bud, and fruits, with the most abundant transcript accumulation in the flower (Figure 1d). We then generated transgenic tomato plants expressing the *GUS* reporter gene under the control of the *SIJUL* promoter. Histochemical *GUS* staining was detected in all of the examined organs (Figure 1e–g, Figure S2). The reporter expression was also visible in the emerging embryonic roots of germinating seeds (Figure S2a). At the later developmental stage, *GUS* staining was observed in all organs, including the pedicel, stamen, style, sepals, and fruits (Figure 1e, f, Figure S2b–d). In particular, the *GUS* signal was localized to the vasculature of the immature green fruits, red ripe fruits, and anthers (Figure 1e–h).

SIJUL functions as a negative regulator of phloem differentiation in tomato

To test the possibility that *SIJUL* functions as a regulator of phloem development, we generated *SIJUL* knockdown lines (hereafter, *TRV-SIJUL*) using a virus-induced gene silencing (VIGS) technique (Figure S3) and compared their vascular anatomy with control tomato plants [*TRV-SIPDS* (*PHYTOENE DESATURASE*) and *TRV-GFP*]. Examination of the cross sections of the peduncles from the control and *SIJUL* knockdown plants revealed that the suppression of *SIJUL* increased the total phloem cell population by 1.77-fold when compared with *TRV-GFP* plants (Figure 2a–b). Consistently, the expression of a phloem marker gene, *ALTERED PHLOEM DEVELOPMENT* (*SIAPL*), was increased by 1.82-fold in *TRV-SIJUL* (Figure 2c), while that of cambium [*TDIF RECEPTOR*

Figure 1 Identification and characterization of the *SIJUL*–*SISMXL* regulatory module. *SIJUL* shares a high degree of similarity with AtJUL1. (a) Schematic of the *SIJUL* and AtJUL1 amino acid sequence alignment. Conserved ZnF domains are underlined and conserved residues are highlighted with different background colours. Conserved 'arginine (R)'s are required for RNA-binding and 'cysteine (C)'s stabilize the finger structure itself. *SIJUL* suppresses the translation of *SISMXL5*. (b) Representative images of *Arabidopsis* protoplasts co-expressing the *SISMXL5* 5' UTR-*GFP* fusion with increasing concentrations of *SIJUL* (top) or *SIJUL*^{R20/R81/R151A} (bottom). The levels of *SIJUL* (anti-HA) and *GFP* proteins in the total protein extracts were determined using an immunoblot, while the *GFP* transcripts were assessed using RT-PCR. These experiments were repeated three times independently with reproducible results. Scale bars, 200 μ m. (c) Reporter assays of the interaction between the *SISMXL5* 5' UTR- or *mSISMXL5* 5' UTR-fused *LUC* with *SIJUL* or *SIJUL*^{R20/R81/R151A}. The values of the *LUC* activities were normalized using the values from the 35S promoter-driven Renilla activity. Data are shown as means \pm s.e.m. ($n = 12$; ns, non-significant). Different letters indicate significantly different statistical groups (Tukey-HSD, $P < 0.05$). These experiments were repeated three times independently with similar results. *SIJUL* is ubiquitously expressed in all plant organs. (d) The qRT-PCR-based quantification of *SIJUL* expression was performed three times independently with similar results. The gene expression values were normalized against expression values of the *GAPDH* reference gene. Data are shown as means \pm s.e.m. ($n = 3$). Different letters indicate significantly different statistical groups (Tukey-HSD, $P < 0.05$). *SIJUL* expression is prominent in vascular tissues. (e–f) *SIJUL* promoter-driven *GUS* signal in (e) transverse section of an immature green fruit and (f) the longitudinal section of a red ripe fruit. Yellow arrows indicate the vasculature. (g) A bright-field image of an anther cross section showing the *GUS* signal in the vasculature. (h) Magnified view of vasculature shown in (g). Black arrows indicate xylem. The cross section in (g) was counter-stained with Safranin-O. Scale bars, 1 cm (e, f), 100 μ m (g).



(TDR)] and xylem [*IRREGULAR XYLEM 3 (IRX3)*] marker genes was unaltered (Figure S4a). We also generated two different stable *sjul* null mutant lines using the CRISPR-Cas9 system (Figure S5 and S6). Like the *TRV-SIJUL* knockdown lines, the transgenic plants containing the *sjul* null alleles exhibited a dramatic proliferation of phloem tissue with a 7.74-fold increase in *SIAPL* marker expression compared with the wild type (Figure 2d–e; Figure S6b). These data demonstrate that the defect in *SIJUL* expression leads to an increment in phloem tissue.

To assess whether the RNA-binding activity of *SIJUL* is necessary for its function in phloem development, we generated tomato plants constitutively expressing mutated *SIJUL^{R20/81/151A}* (*35S:SIJUL^{R20/81/151A}*) (Figure 2f). Intriguingly, the transgenic tomato plants expressing *SIJUL^{R20/81/151A}* also displayed a drastic increase of 1.84-fold in their phloem cell population and an enhanced expression of *SIAPL* with a 3.14-fold increase over wild type control (Figure 2g, h). We assume that *SIJUL^{R20/81/151A}* functions as a dominant-negative form of *SIJUL* probably

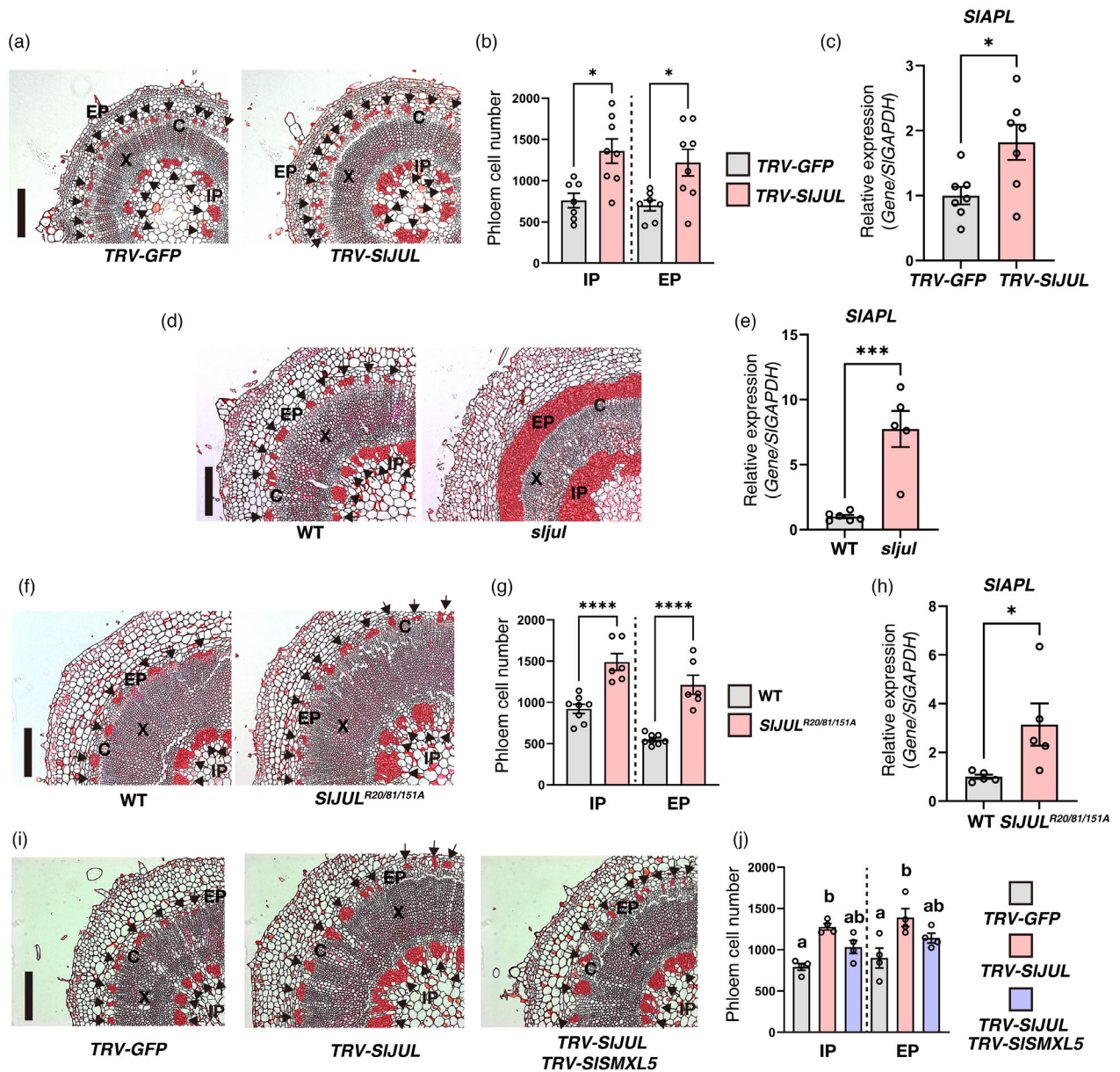


Figure 2 Functional characterization of *SIJUL*. Knockdown or knockout of *SIJUL* enhanced phloem tissues. The peduncles from the presented plant were cross sectioned at 30-days-post-anthesis (dpa) of the first raceme. (a) Representative images of peduncle cross sections from *TRV-GFP* and *TRV-SIJUL* plants at 8-weeks post infiltration. Black arrows indicate phloem. Scale bar, 100 μ m. (b) Quantification of phloem cell number in *TRV-GFP* and *TRV-SIJUL*. Data are shown as means \pm s.e.m. (n is at least 7; $*P < 0.05$, determined using a two-tailed Student's t -test). IP is inner phloem; EP is external phloem, C is cambium; X is xylem. (c) Expression of *SIAPL*, a phloem marker gene. The expression value of the gene was normalized against expression values of the *GAPDH* reference gene. Data are shown as means \pm s.e.m. ($n = 7$; $*P < 0.05$, determined using a two-tailed Student's t -test). All these experiments were repeated three times independently with similar results. (d) Representative bright-field images of the peduncle cross sections from the WT and *sjul*-Cas9 plants. Black arrows indicate phloem. IP is inner phloem; EP is external phloem, C is cambium; X is xylem; WT is wild type. Scale bars, 100 μ m. (e) Expression of *SIAPL* in the WT and *sjul*-Cas9. The expression value of the gene was normalized against expression values of the *GAPDH* reference gene. These experiments were repeated three times independently with similar results. Data are shown as means \pm s.e.m. (n is at least 5; $***P < 0.001$, determined using a two-tailed Student's t -test). Conserved 'R's in the ZnF domains of *SIJUL* are critical for its role in phloem development. (f) Representative images of peduncle cross sections showing increased phloem tissue in the plants constitutively expressing *SIJUL*^{R20/81/151A}, a mutant form of *SIJUL* (35S:*SIJUL*^{R20/81/151A}) compared with WT plants. Black arrows indicate phloem. Scale bar, 100 μ m. (g) Phloem cell numbers in the WT and *SIJUL*^{R20/81/151A} plants. Data are the means \pm s.e.m. ($n = 6$; $*P < 0.05$, determined using a two-tailed Student's t -test). (h) Expression of *SIAPL* in the WT and *SIJUL*^{R20/81/151A} plants. The expression value of the gene was normalized against expression values of the *GAPDH* reference gene. Data are shown as means \pm s.e.m. ($n = 5$; $*P < 0.05$, determined using a two-tailed Student's t -test). *SIJUL* acts upstream of *SISMXL5* and suppresses the latter to effectuate phloem development. (i) Representative images of peduncle cross sections of *TRV-GFP*, *TRV-SIJUL*, and *TRV-SIJUL/TRV-SISMXL5* tomato plants. Black arrows indicate phloem. Scale bar, 100 μ m. (j) Phloem cell count in the *TRV-GFP*, *TRV-SIJUL*, and *TRV-SIJUL/TRV-SISMXL5* plants. Data are the means \pm s.e.m. ($n = 4$). Different letters indicate significantly different statistical groups (Tukey-HSD, $P < 0.05$). All these experiments were repeated three times independently with similar results.

competing with wild-type *SIJUL* for binding to the target G-quadruplexes *in planta*. Next, we suppressed the expression of *SISMXL5*, a target of *SIJUL* in phloem development, in the *SIJUL* knockdown plants using VIGS, which decreased the population of total phloem cells in the *TRV-SIJUL* tomato and partially restored the phloem cells to the levels in the control plants (Figure 2i, j). These results demonstrate that *SIJUL* is an evolutionarily conserved negative regulator of phloem differentiation in tomato and support the functional relevance of the *SIJUL-SISMXL5* regulatory module in phloem differentiation *in planta*.

The level of *SIJUL* suppression dictates plant growth attributes

To ascertain whether the anatomical change in the plant vasculature caused by the suppression of *SIJUL* is manifesting the plant morphology or growth attributes, we recorded various growth parameters in knockdown (*TRV-SIJUL*), suppression (*35S:SIJUL^{R20/81/151A}*), and knockout (*sljul-Cas9*) plants. The number of leaves, stem diameter, and the leaf area were unchanged in *TRV-SIJUL* (Figure 3a–c) and *35S:SIJUL^{R20/81/151A}* (Figure 3i–k) over their respective control plants. Likewise, the flower number, leaf photosynthetic efficiency, and CO₂ assimilation rate of both these lines were similar to the control plants (Figure 3d–h, l, n–p). By contrast, the *sljul-Cas9* knockout plants exhibited a significant reduction in leaf number and area, stem diameter and flower number (Figure 3q–t). Intriguingly, the peduncle length, a measure of phloem path between source and the sink, was decreased in both *35S:SIJUL^{R20/81/151A}* and *sljul-Cas9* plants (Figure 3m, u). The photosynthetic efficiency and CO₂ assimilation rates of the source leaves from all three lines remained unchanged (Figure 3w–x). However, the reduced number of the photosynthesizing organs combined with unchanged CO₂ assimilation implies an overall reduction in the net carbon assimilation in *sljul-Cas9* plants. Altogether, the contrasting results on plant growth attribute in knockdown plants with an optimal increment in the phloem tissue and the knockout plants bearing prolific phloem tissue indicate that phloem hyperplasia is limiting to plant growth attributes in tomato.

Increment in phloem tissue confers rapid transport capacity

To determine whether the increased phloem cells affect the phloem transport capacity, we delineated the transport traits in the source leaves responsible for supplying photoassimilates to the fruit truss in *SIJUL* knockdown and knockout plants. We monitored the transport of an ultraviolet fluorescent dye, esculin. Esculin is a sucrose analogue, specifically loaded into the phloem stream by the members of the *SUCROSE TRANSPORTER (SUT)* family and thereby used to trace phloem transport (Knoblauch *et al.*, 2015; Knox *et al.*, 2018; Rottmann *et al.*, 2018). The knockdown and knockout tomato plants have increased phloem cells in the source leaf petiole (Figure 4c, g, k) and showed an enhanced esculin loading into the leaf vasculature when compared with the control (Figure 4a–b, e–f, i–j). We then estimated phloem transport velocity and export rate of esculin in the midrib of leaves. Esculin reached the base of the midrib within 10 min in *TRV-SIJUL* leaves but took about 35 min in *TRV-GFP* leaves (Figure S7a). However, the export rate was not significantly altered in *TRV-SIJUL* lines when compared with control (Figure S7b–d). Thus, it is likely that the enhanced esculin transportation observed in *TRV-SIJUL* lines was due to increased vascular

loading achieved within the first 10 min. The mechanism of active phloem (un)loading involves sugar transporters. The *SUT* and the *SUGARS WILL EVENTUALLY BE EXPORTED TRANSPORTERS (SWEET)* families play a critical role in the export of photosynthetically fixed carbon from source leaves and the reloading of sucrose into the phloem continuum or the import of sucrose into the sink organs, such as fruits (Hackel *et al.*, 2006; Ru *et al.*, 2020; Shammai *et al.*, 2018). Thus, we examined the transcript levels of the key genes involved in sucrose transport in the source leaf using qRT-PCR. The transcript levels of *SISUT1*, *SISUT2*, *SISUT4* (Reuscher *et al.*, 2014), and *SISWEET1a* (Ho *et al.*, 2019) exhibited a significant increase by 1.66, 1.62, 1.78, and 1.36 fold, respectively, in the *TRV-SIJUL* tomato leaves compared with the *TRV-GFP* plants (Figure 4d). The *35S:SIJUL^{R20/81/151A}* plants exhibit a 3.54-fold increase and *sljul-Cas9* plants exhibit a 3.83-fold increase in *SUT1* expression when compared with their respective wild-type plants (Figure 4h, l). Since the long-distance transport is also influenced by sieve element length and radius (Damari-Weissler *et al.*, 2009; Lucas *et al.*, 2013), we measured these features from the longitudinal sections of *TRV-SIJUL* and *TRV-GFP* plants. As per the observations, we did not find any measurable differences in the dimensions of sieve tubes in the two plants (Figure S8). These data indicate that the increased phloem cell population in the *SIJUL* knockdown and knockout plants augmented the phloem transport capacity.

Phloem threshold governs fruit sink strength in tomato

To examine whether the increased phloem flow directly affects the yield, we measured the mean fruit number, fruit size, and fruit weight per plant. The *TRV-SIJUL* knockdown plants exhibited a significant increase of 37% in fruit numbers with no measurable difference in fruit size over *TRV-GFP* (Figure 5a–c). The value on increased fruit number contributed to a remarkable increase of 60% in total fruit weight in *TRV-SIJUL* (Figure 5d). Further to assess whether the *SIJUL*-mediated influence on fruit yield is asserted through its target *SISMXL5*, we silenced *SISMXL5* (using *TRV-SMXL5*) in the *TRV-SIJUL* background (to make *TRV-SISMXL5/TRV-SIJUL* plants) (Figure 5a–d). Upon silencing of *SISMXL5*, the *SIJUL* knockdown effects on increased yield now returned to the levels comparable to *TRV-GFP* control in *TRV-SISMXL5/TRV-SIJUL* plants (Figure 5a–d). Not only, but the total sugar content in *TRV-SIJUL* fruits was also increased up to 25% compared with *TRV-GFP* fruits. *TRV-SIJUL* fruits had 28% and 22% higher glucose and fructose contents, respectively than the *TRV-GFP* fruits (Figure S9). Our results show that the increased phloem cell population resulting from the suppression of *SIJUL* expression enhanced sink strength in tomato. Unexpectedly, the *35S:SIJUL^{R20/81/151A}* plants displayed a 51% increase in fruit numbers but bore smaller fruits when compared with wild-type plants (Figure 5e–g). The resultant yield measured as the mean fruit weight per plant thus remained unchanged in *35S:SIJUL^{R20/81/151A}* plants (Figure 5h). The noted increment in fruit numbers in the *TRV-SIJUL* plants could be attributed to the reduced rate of flower/fruitlet abortion in these plants compared with *TRV-GFP* plants (Figure S10a). Such a phenomenon could be explained by the increased rate of photoassimilate allocation at the onset of inflorescence sink in the *SIJUL* knockdown plants. Unlike the knockdown plants, *sljul-Cas9* knockout plants bore a drastically reduced number of fruits which is consistent with the compromised plant growth and reduced number of flowers. The fruits, however, were bigger, when compared with the wild-type plants

(Figure 5I–I). These data demonstrate a likely trade-off between fruit number per plant and mean fruit size reflective of the increased sink competition for photoassimilates. Further, to validate if the increased number of fruits clamour for resource allocation, we pruned the tomato plants to reduce competition and achieve a potential fruit growth condition in which fruit growth was not compromised. In this respect, we adjusted the per plant fruit number to 10 in both the *TRV-SIJUL* and the control *TRV-GFP* and recorded the fruit size and weight as a measure of sink biomass (Figure 510b). In *TRV-SIJUL*, the size and weight of the fruits were significantly increased by up to 24% and 66%, respectively, compared with the *TRV-GFP* fruits (Figure 510c–e). Therefore, the ‘sink strength’ here reflects the potential for biomass gain, when the left-over *TRV-SIJUL* fruits after pruning or the sparse *sljul-Cas9* fruits displayed a potential to accumulate more biomass. Though our results suggest a correlation between the phloem increment and increased transport capacity, the fruits were resource supply limited rather than sink strength limited.

Discussion

The homeostasis between the efficiency of carbon fixation at the source and carbon allocation to the sink is tightly coordinated to regulate developmental and stress-adaptive processes (Ruan, 2014). This photoassimilate partitioning is influenced by (1) the efficiency of resource acquisition by source organ (D’Aoust *et al.*, 1999; Micallef *et al.*, 1995), (2) the transport of resources from source to sink (Hackel *et al.*, 2006), and (3) resource utilization at the sink (Osorio *et al.*, 2014). In recent years, increasing the photosynthetic efficiency as a mean of increasing photosynthate partitioning into the sink (harvestable) organs was explicitly used by breeders to select for high-yielding crops (Betti *et al.*, 2016; Cormier *et al.*, 2016; Gifford *et al.*, 1984; Murchie and Niyogi, 2011; Price *et al.*, 2008). Invariable photosynthetic activity in the source and the signalling networks in plant productivity exerts a limit for the allocation of carbon and nitrogen in plants (Yu *et al.*, 2015). Similarly, the enforcement of sugar partitioning into sink organs by an increase in local unloading impairs their homeostasis with source organs, leading to a disadvantage in growth properties (Dasgupta *et al.*, 2014). We, therefore, hypothesized that it would be possible to enhance the distribution of photosynthates across sink organs by governing phloem development.

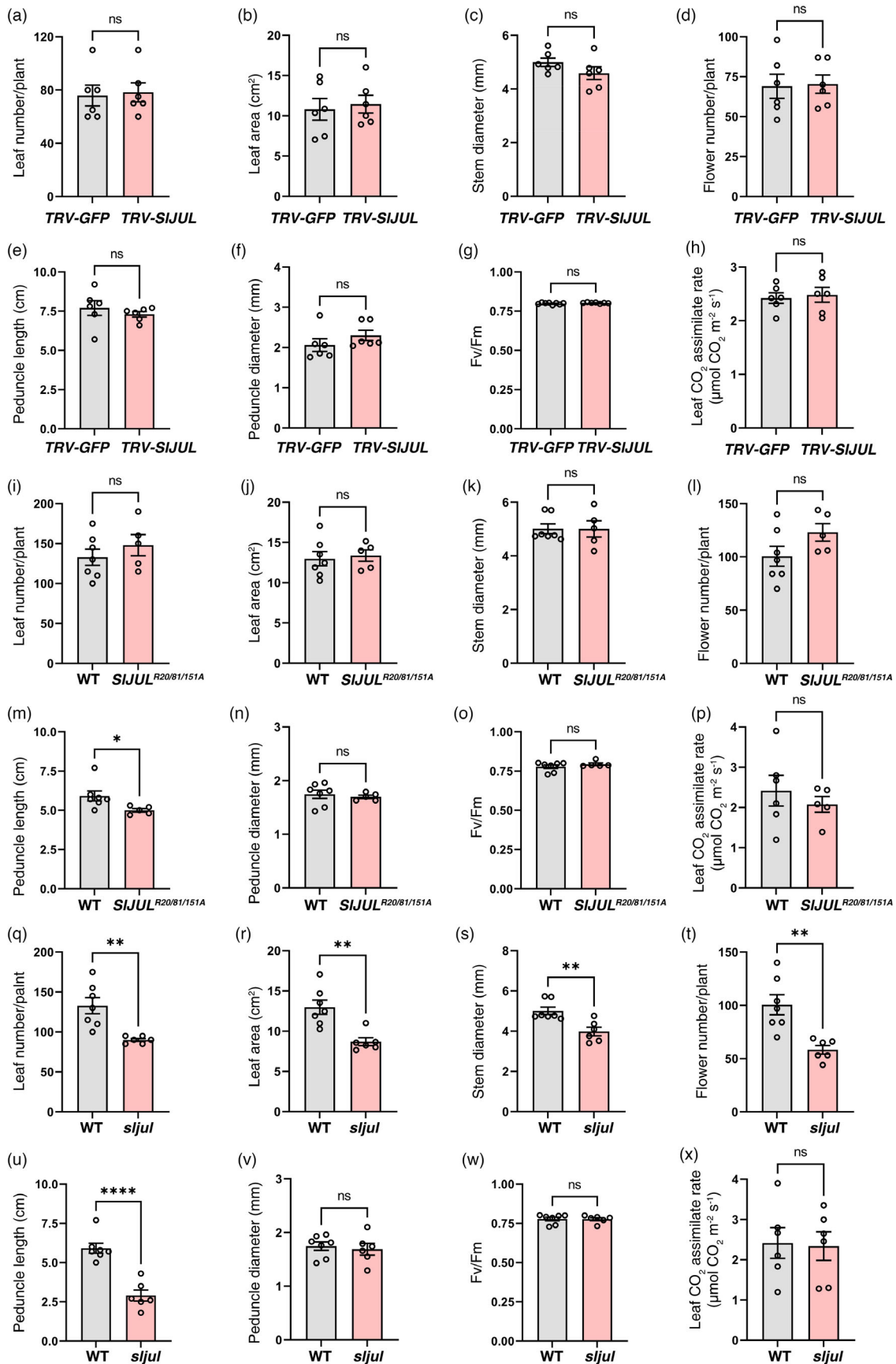
Though phloem tissue is the primary continuum driving photoassimilate partitioning, the developing sink is the key determinant of phloem transport (Kallarackal and Milburn, 1984; Lucas *et al.*, 2013). However, the relationship among the phloem cell population, the efficiency of resource partitioning, and sink strength remains poorly understood. Here, we identified

and characterized the *SIJUL-SISMXL5* regulatory module for phloem development *in planta*. The *SIJUL* knockdown invoked increments in phloem cells associated with the rapid phloem loading that without compromising growth and developmental traits led to increased fruit yield. These changes were however reverted to control levels when *SISMXL5* was silenced in *TRV-SIJUL* background (*TRV-SISMXL5/TRV-SIJUL*), hence providing the biotechnological implication of the *SIJUL-SISMXL5* module in controlling fruit yield and establishing a positive correlation between the rate of phloem transport and yield potential of tomato.

With overexpression of the *SIJUL*^{R20/81/151A} form, the number of fruits was increased, though the total yield in terms of fruit weight per plant remained unchanged. In yet another scenario, the *sljul* null allele (*sljul-Cas9*) invoked substantive increment in phloem cell number along with an enhanced rate of phloem transport and increased expression of genes encoding sugar transporters, exhibited reduced fruit numbers with increased mean fruit size than that of wild-type plants. Altogether, our results implicate a trade-off between fruit size and fruit number when a plant (a) is equipped with a rapid system to transport assimilates from source to fruit sink, but (b) exhibits invariable resource acquisition at the source (photosynthetic efficiency). Based on the comparative results, we suggest that the rate of phloem transport is the key determinant of plant growth and sink strength under limiting resource acquisition (Figure 511). Engineering an efficient phloem transport system thus seems a viable approach for strengthening the overall sink, thereby facilitating crop improvement.

In this work, we employed two different approaches to silence *SIJUL* expression: The first strategy involved the VIGS-mediated transient knockdown of *SIJUL* to validate its functional relevance in phloem development and transport, and the second strategy used CRISPR-Cas9 to silence *SIJUL* expression in stable transgenic plants. Intriguingly, with the VIGS-mediated reduction of *SIJUL* expression, we did not find any measurable abnormalities in the plant growth attributes. On the contrary, the CRISPR-Cas9-mediated complete silencing of *sljul* led to considerable stunting of plant height (Figure 5i, Figure 56d). The evident differences in the morphologies of the *TRV-SIJUL* and *sljul-Cas9* plants could either be due to the reduction of *SIJUL* expression at different stages of plant ontology or the differences in the overall level of *SIJUL* suppression between the two genotypes. It is thus necessary to develop an optimal system for the controlled manipulation of *SIJUL* expression to revamp the phloem cell population and increase yield traits without compromising plant growth. To achieve this, promoter engineering and base editing using CRISPR-Cas9 could be considered (Kang *et al.*, 2019; Kwon *et al.*, 2020; Mishra *et al.*, 2020; Rodríguez-Leal *et al.*, 2017; Shimatani *et al.*, 2017), or tissue- or organ-specific promoters

Figure 3 Morphology and growth parameters in *SIJUL* knockdown and knockout tomato plants. *SIJUL* knockdown (*TRV-SIJUL*) or constitutively expressing *SIJUL*^{R20/81/151A} (*35S:SIJUL*^{R20/81/151A}) does not hamper plant growth traits. Various phenotypic observations were recorded from 30 dpa plants: (a) (i) average leaf number; (b), (j) leaf area; (c), (k) stem diameter; (d), (l) flower number; (e), (m) peduncle length; (f), (n) peduncle diameter; (g), (o) source leaf photosynthetic efficiency, and (h), (p) CO₂ assimilation rates of source leaf. Data are shown as means ± s.e.m, (*n* is at least 6; ns, non-significant; **P* < 0.05, determined using a two-tailed Student’s *t*-test). All these data were recorded three times independently with similar results. The *sljul* knockout plants exhibit restricted growth. The observations were recorded from WT and *sljul-Cas9* plants at 30 dpa of the first raceme: (q) average leaf number; (r) leaf area; (s) stem diameter; (t) flower number; (u) peduncle length; (v) peduncle diameter; and (w) Chlorophyll fluorescence (Fv/Fm) of PHOTOSYSTEM II (PSII) as a measure of the source leaf photosynthetic efficiency and (x) CO₂ assimilation rates of source leaf. Data are shown as means ± s.e.m, (*n* is at least 6; ns, non-significant; ***P* < 0.01, *****P* < 0.0001, determined using a two-tailed Student’s *t*-test).



could be used to drive *JUL* expression in a spatiotemporal manner without causing any pleiotropic effects on plant growth. However, a clear understanding of the probable correlation between crop productivity and the regulation of *SIJUL* expression and its activity in controlling the phloem cell population to varying degrees is still lacking and should be a subject for future studies.

Notably, the stunted plant trait with enhanced phloem flow could have potential in vertical farming, where more recently a compact plant architecture trait has been aggressively exploited by breeders in urban farms. If the traits regulated by *JUL* can be suitably translated into leafy greens, herbs, and plants exploited for molecular farming, the more compact size would allow more crops to be grown in a limited space. Although it is necessary to confirm whether the yield per hectare is further increased by utilizing this trait, this study demonstrated a new crop productivity strategy based on the enhanced energy distribution beyond the limitations of the existing strategy.

Experimental procedures

Plant material and growth conditions

Seeds of the tomato cultivar Micro-Tom were provided by Do-il Choi at Seoul National University, Seoul, Republic of Korea. All seeds were germinated on media (pH 5.7) containing half-strength Murashige and Skoog salts including vitamins (Duchefa), 3% sucrose (Duchefa), 0.5% 2-(*N*-morpholino)ethanesulfonic acid (MES; Sigma-Aldrich), and 0.8% phytoagar (Sigma-Aldrich) under long-day conditions (16 h light/8 h dark), 1200 $\mu\text{mol s}^{-1} \text{m}^{-2}$ light intensity and 24 °C growth temperature. At 10 days after sowing (DAS), the seedlings were transplanted into pots and grown under long-day conditions. The *Arabidopsis thaliana* ecotype Col-0 grown under short-day conditions (8 h light/16 h dark) was used for the protoplast experiments.

Plasmid construction and tomato genetic transformation

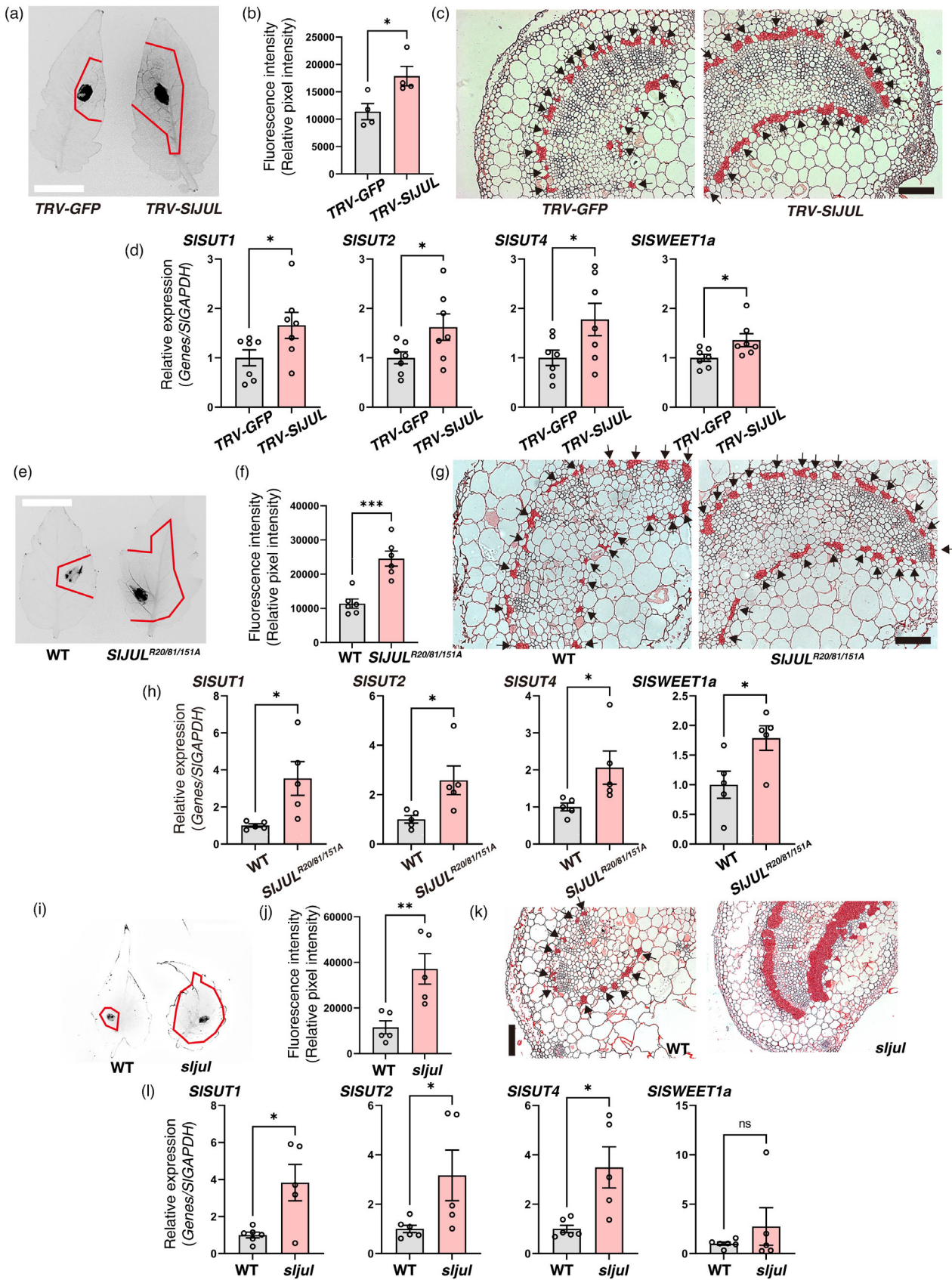
For the VIGS assay, the off-target free cDNA fragments of *SIJUL* (*Solyc08g067180.3.1*; 214 bp) and *SISMXL5* (*Solyc07g018070.3.1*; 549 bp) (<https://www.zhaolab.org/pssRNAit/>) were amplified using cDNA templates derived from Micro-Tom

tomato and cloned into the *pTRV2* vector (*pYL156*, Addgene plasmid # 148969; <http://n2t.net/addgene:148969>). For the protoplast reporter assay, the 5' UTR of *SISMXL5* (336 bp) was cloned into the plant expression vector harbouring either *GFP* or *LUC* (*35S:SISMXL5* 5' UTR-*GFP*, *35S:SISMXL5* 5' UTR-*LUC*, and *35S:mSISMXL5* 5' UTR-*LUC*), and the full-length coding sequence (CDS) of *SIJUL* (513 bp) was cloned into the plant expression vector containing a hemagglutinin (HA) tag (*35S:SIJUL::HA*). The point mutations in *SIJUL* [R20(AGA)(58,59,60)→A(GCA), R81 (CGC)(241,241,243)→A(GCC), and R151(AGG)(451,452,453)→A(GCG)] to create *SIJUL*^{R20/81/151A} and in the *SISMXL5* 5' UTR (*mSISMXL5* 5' UTR) were generated using the QuikChange Site-Directed Mutagenesis Kit (Stratagene California).

To elucidate the spatial expression pattern of *SIJUL*, the 2.0 kbp sequence upstream of the translation start site was amplified from the Micro-Tom tomato genomic DNA (isolated using the CTAB method following the published protocol (Murray and Thompson, 1980) and cloned into *pCAMBIA1303* (*SIJUL::GUS-GFP*). The full-length CDS of *SIJUL* containing point mutations was introduced in the *pBI121* binary vector containing the *CaMV 35S* promoter (*Cauliflower mosaic virus*) and a *GUS* fusion sequence to generate the *35S:SIJUL*^{R20/81/151A} *GUS* construct.

To generate the CRISPR knockouts, sgRNAs were designed using the CRISPR-P 2.0 tool (Liu *et al.*, 2017) and used for CRISPR vector construction. All the T-DNA constructs used in this study were based on the Gateway-compatible *pEn-C1.1* (Holger Puchta, Addgene plasmid #61479; <http://n2t.net/addgene:61479>) and *pDe-CAS9* (Holger Puchta, Addgene plasmid #61433; <http://n2t.net/addgene:61433>) plasmids. The destination vector *pDe-CAS9* expresses *Cas9* driven by the constitutive *PcUbi4-2* promoter [*Ubiquitin* promoter from parsley (*Petroselinum crispum* Miller)] and contains the terminator sequence of pea (*Pisum sativum* L.) small subunit of RIBULOSE-1,5-BISPHOSPHATE CARBOXYLASE (*RBCS3A*, *pea3A*) gene. Spacer sequences (20 bp) were introduced into the entry vector as annealed oligonucleotides using classical cloning by restricting the sequences using *BbsI* (New England Biolabs). The customized RNA chimera is driven by the *Arabidopsis U6-26* promoter. For the simultaneous targeting of two different positions (5' UTR and 3' UTR) in *SIJUL*, two programmed sgRNA cassettes were integrated

Figure 4 Phloem transport capacity of *SIJUL*-suppressed plants. The increased phloem tissues due to *SIJUL* knockdown and knockout enabled a higher rate of sugar transport quantified in source leaves supporting the first raceme in plants at 30 dpa. Data for *TRV-SIJUL* knockdown plants showing (a) Representative UV transilluminator images of the fluorescence observed 10 min after loading the esculin. Scale bar, 1 cm. (b) Quantification of the esculin transport in the source leaves. Data are shown as means \pm s.e.m, ($n = 4$; $*P < 0.05$, determined using a two-tailed Student's *t*-test). (c) Images of the petioles cross sections of the corresponding leaves showing increased phloem tissues in *SIJUL* knockdown plants (*TRV-SIJUL*) relative to the negative control, *TRV-GFP*. Scale bar, 100 μm . Black arrows indicate phloem. (d) Relative expression of the key genes encoding sucrose transporters in source leaves from *TRV-SIJUL* and *TRV-GFP* plants, normalized against expression values of the *GAPDH* reference gene. Data are shown as means \pm s.e.m, ($n = 7$; $*P < 0.05$, determined using a two-tailed Student's *t*-test). These experiments were repeated three times independently with reproducible results. Data from stable suppression of *SIJUL* (*SIJUL*^{R20/81/151A}) lines showing (e) Representative UV transilluminator images of the fluorescence observed 10 min after loading the esculin. Scale bar, 1 cm. (f) Quantification of the esculin transport in the source leaves. Data are shown as means \pm s.e.m, ($n = 6$; $***P < 0.001$, determined using a two-tailed Student's *t*-test). (g) Cross section images of the petioles of the corresponding leaves showing increased phloem tissues in *SIJUL*^{R20/81/151A} relative to the negative control, WT. Scale bar, 100 μm . Black arrows indicate phloem. (h) Relative expression of the key genes encoding sucrose transporters in the source leaves from WT and *SIJUL*^{R20/81/151A} plants, normalized against expression values of the *GAPDH* reference gene. Data are shown as means \pm s.e.m, ($n = 5$; $*P < 0.05$, determined using a two-tailed Student's *t*-test). These experiments were repeated three times independently with reproducible results. The increased phloem tissues of the stable *sljul* null allele enabled a higher rate of sugar transport. (i) Representative UV transilluminator images of the fluorescence observed 10 min after loading the esculin. Scale bar, 1 cm. (j) Quantification of the esculin transport in the source leaves. Data are shown as means \pm s.e.m, ($n = 6$; $***P < 0.001$, determined using a two-tailed Student's *t*-test). (k) Cross sections of the petioles of the corresponding leaves showing increased phloem tissues in *sljul-Cas9* relative to the negative control, WT. Scale bar, 65 μm . Black arrows indicate phloem. (l) Relative expression of the key genes encoding sucrose transporters in the source leaves from WT and *sljul-Cas9* plants, normalized against expression values of the *GAPDH* reference gene. Data are shown as means \pm s.e.m, (n is at least 5; ns, non-significant; $*P < 0.05$, determined using a two-tailed Student's *t*-test). These experiments were repeated three times independently with reproducible results.



into the destination vector. The first chimera was transferred using *Bsu36I* and *MluI* (New England Biolabs), and the second chimera was transferred using a Gateway LR reaction (Thermo Fischer Scientific), as previously described (Schiml *et al.*, 2014).

To generate another CRISPR knockout allele, the sgRNA was designed to target ZnF motif 1 and 2 sequences in the *SIJUL*. The T-DNA constructs used here were based on the *pHAtC* (Jin-Soo Kim, Addgene plasmid #78098; <https://www.addgene.org/78098>) plasmid. The *pHAtC* expresses *Cas9* driven by the 35S promoter and the customized RNA chimera is driven by the *Arabidopsis U6-26* promoter. Spacer sequence (20 bp) was introduced into the plant transformation vector as annealed

oligonucleotides using classical cloning by restricting the sequences using *AarI* (Thermo Fischer Scientific). The sgRNA cloning primer sets used in this study are listed in Table S1.

The final binary plasmids were introduced into the cotyledons explants of 10 DAS seedlings (tomato cultivar Micro-Tom) using *Agrobacterium tumefaciens* (strain EHA105)-mediated transformation, as described previously (Sun *et al.*, 2006). Tomato transformants were selected on BASTA (1 mg/L; Bayer Crop Science) or hygromycin (5 mg/L; Duchefa). T2 generation of the transgenic 35S:*SIJUL*^{R20/81/151A} and *sljul*-*Cas9* lines were used for further studies. All the primers used in this study are detailed in Table S1.

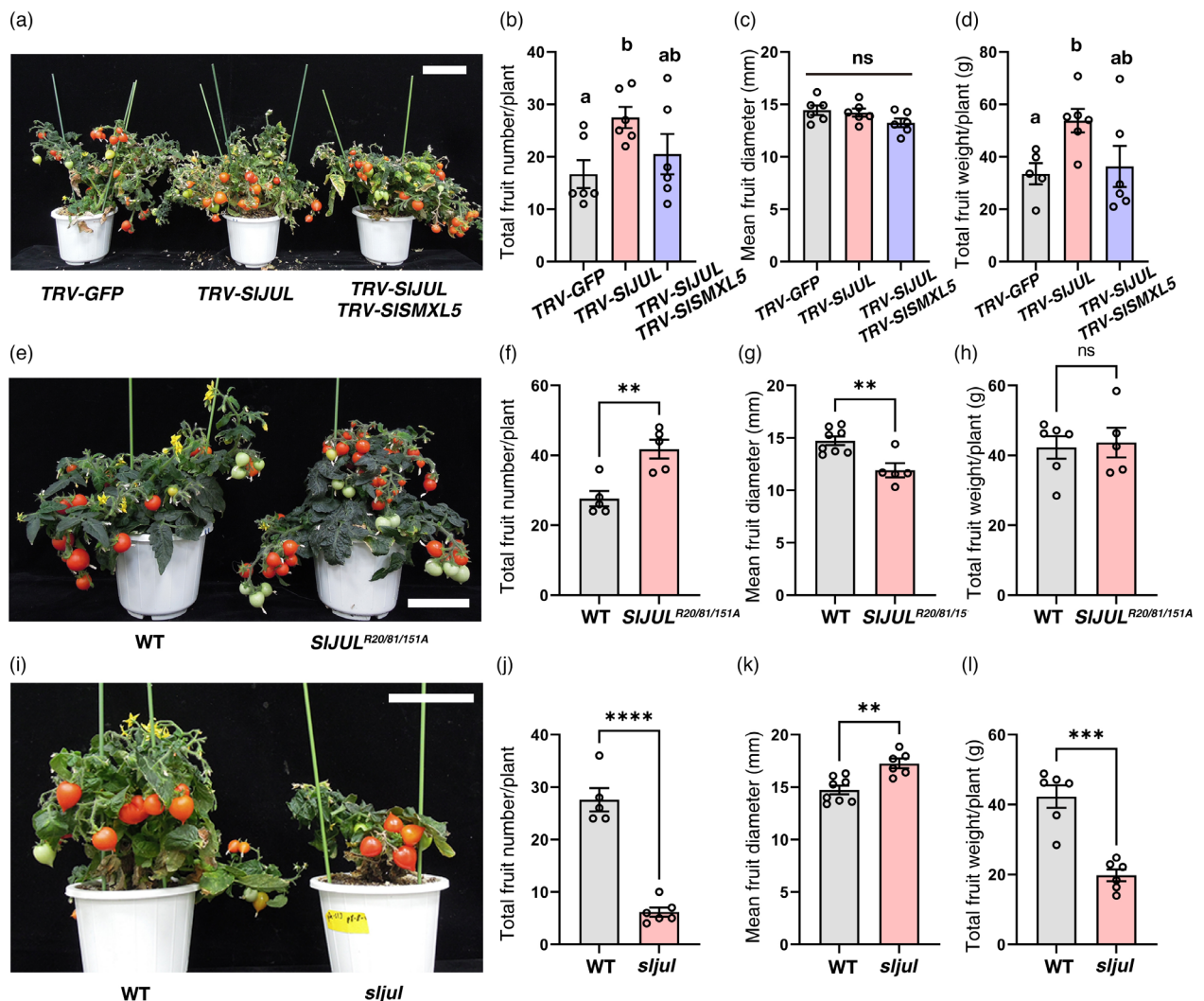


Figure 5 Characterization of the fruit sink strength in *SIJUL*-suppressed plants. *SIJUL* knockdown invoked a higher rate of fruit set. (a) Representative images of 60 dpa *SIJUL* knockdown plants (*TRV-SIJUL*), *SIJUL* and *SISMXL5* knockdown plants (*TRV-SISMXL5/TRV-SIJUL*) and the negative control, *TRV-GFP*. Scale bar, 10 cm. (b) Average fruit number (c) mean diameter of red ripe fruits and (d) total fruit weight per plant in *TRV-GFP*, *TRV-SIJUL* and *TRV-SISMXL5/TRV-SIJUL* plants. Data are shown as means \pm s.e.m. ($n = 6$; ns, non-significant). Different letters indicate significantly different statistical groups (Tukey-HSD, $P < 0.05$). These experiments were repeated three times independently with similar results. For the mean fresh weight of fruit per plant, all the fruits (irrespective of the stage) were accounted at 60 dpa of the first raceme. (e) Representative images of WT and *SIJUL*^{R20/81/151A} plants. Scale bar, 10 cm. (f) Average fruit number (g) mean fruit diameter and (h) total fruit weight per plant in WT and *SIJUL*^{R20/81/151A} plants. Data are shown as means \pm s.e.m. (n is at least 5; ns, non-significant; ** $P < 0.01$, determined using a two-tailed Student's *t*-test). *SIJUL* knockout (*sljul*-*Cas9* null allele) leads to a reduced rate of fruit set. (i) Representative images of WT and *sljul*-*Cas9* plants at 60 dpa. Scale bar, 10 cm. (j) Average fruit number (k) mean fruit diameter and (l) total fruit weight per plant in WT and *sljul*-*Cas9*. Data are shown as means \pm s.e.m. (n is at least 5; ** $P < 0.01$, *** $P < 0.001$, **** $P < 0.0001$ determined using a two-tailed Student's *t*-test).

Protoplast preparation, transient expression assay, and immunoblotting

Fully expanded leaves of 3- to 4-week-old *Arabidopsis* plants were used for the protoplast isolation. Mesophyll protoplasts and plasmid DNA were prepared following the published protocol (Hwang and Sheen, 2001). For the reporter assay, the protoplasts were diluted to a density of 2×10^4 cells/mL and transfected with 20 μ g of plasmid DNA composed of different combinations of the reporters (*SISMXL5* 5' UTR-*GFP*, *SISMXL5* 5' UTR-*LUC*, or *mSISMXL5* 5' UTR-*LUC*), effectors (*35S:SIJUL::HA* or *35S:SIJUL^{R20/81/151A}::HA*), and internal control (*35S:Renilla* for luciferase assay). The transfected protoplasts were incubated for 6 h at room temperature. For the reporter assay, the relative activity of each gene was measured using a dual luciferase assay with the firefly luciferase assay system (Promega) and the Renilla luciferase assay system (Promega).

To detect the target protein levels, the total protein was extracted using protein extraction buffer [50 mM Tris-HCl (pH 7.5), 100 mM NaCl, 5 mM EDTA, 1 mM dithiothreitol, 1x protease inhibitor cocktail (Roche), and 1% Triton X-100]. Subsequently, the extracted proteins were separated using SDS-PAGE on 8–10% polyacrylamide gels, transferred to a nitrocellulose membrane, and immunodetected using anti-HA (for detecting *SIJUL::HA*; 1:2000; Roche) or anti-GFP (for detecting *SISMXL5* 5' UTR-*GFP*; 1:2000; Santa Cruz) antibodies. The levels of the Rubisco large subunit (RbL) were used as the loading control.

Confocal analysis

To determine the subcellular localization of *SIJUL* and *SIJUL^{R20/81/151A}*, their CDSs were cloned into a vector containing the *35S* promoter to generate the *35S:SIJUL-GFP* and *35S:SIJUL^{R20/81/151A}-GFP* constructs, respectively, which was transiently expressed in protoplasts. The fluorescent GFP signals were visualized and photographed under a confocal laser scanning microscope (LSM 800; Carl Zeiss). The fluorescence signals of the chlorophyll and 4',6-diamidino-2-phenylindole (DAPI)-stained nuclei were used to determine cytoplasmic or nuclear positions, respectively, of the target proteins. GFP was excited using a 488-nm wavelength and the emission wavelength was detected between 500 and 550 nm. Chlorophyll was excited using a 640-nm wavelength laser, with emission spectra detected between 650 and 700 nm. For the DAPI fluorescence detection in the protoplasts, 10 μ M DAPI (Sigma-Aldrich) was applied to the sample for 10 min, and an excitation wavelength of 405 nm and emission wavelengths between 420 and 470 nm were used.

Histochemical staining (GUS)

The GUS staining of different organs was conducted as described previously (Millar and Gubler, 2005). Images of GUS-stained tissues/organs were captured using a digital camera mounted on an Axioplan 2 microscope (Carl Zeiss) or Stemi SV 11 Apo stereoscope (Carl Zeiss).

Histological embedding, sectioning, and imaging

The peduncle, petiole, and anther samples were fixed in FAA fixative (3.7% formaldehyde, 5% acetic acid, and 50% ethanol) at 4 °C for 16 h, dehydrated, and embedded in paraffin wax (Paraplast; Leica Microsystems). The fixed samples were sliced into 5 μ m thin sections using a Leica RM2265 microtome (Leica Biosystems). The sections were mounted onto poly-L-lysine-

coated slides and stained with 0.1% safranin O. The micrographs were captured using an Axioplan 2 microscope. Measurements and counting were performed using ImageJ software (NIH; <https://imagej.nih.gov/ij>). The peduncle was sampled at 30-days-post-anthesis (dpa) of the first raceme when the peduncle has completed its vascular development. The petioles correspond to the source leaf subtending to the first raceme.

Virus-induced gene silencing

pTRV2-derived recombinant constructs were transformed into the *A. tumefaciens* strain GV3101. *A. tumefaciens* cultures containing *pTRV1* (*pYL192*; Addgene plasmid # 148968; <http://n2t.net/addgene:148968>) or *pTRV2* constructs were incubated overnight at 28 °C ($OD_{600} = 0.6$), harvested, and resuspended in 10 mM MES (pH 5.5). *Agrobacterium* virulence was induced by adding 100 μ M acetosyringone to the culture suspension and incubating for 3 h at room temperature. *A. tumefaciens* cells ($OD_{600} = 1.0$) containing *pTRV1* or *pTRV2* were mixed in a 1:1 ratio and infiltrated into the leaves of 3-week-old tomato plants. Depending on the nature of the phenotypic or anatomical recordings, the experiments were performed at ~6 weeks after *Agrobacterium* inoculation (30 dpa). To rule out the possible effects of TRV infection, the target gene-silenced plants were compared with plants co-inoculated with *pTRV-GFP* and *pTRV1* as vector control. As a positive control for the VIGS experiment, the silencing effects on the *PHYTOENE DESATURASE (SIPDS)* gene (*pTRV-PDS*) were monitored (Figure S3).

qRT-PCR

Total RNA from the peduncles or leaves of 60-d-old plants was isolated using TRIzolTM reagent (Thermo Fisher Scientific), following the manufacturer's instructions. Reverse transcription was carried out using 1 μ g total RNA, oligo(dT) primers, and ImProm-II reverse transcriptase (Promega). The qRT-PCR was performed following the instructions provided for the StepOnePlus Real-Time PCR system (Thermo Fisher Scientific) with the SYBR Premix ExTaq system (Takara Bio). The expression values of *GLYCERALDEHYDE PHOSPHATE DEHYDROGENASE (SIGAPDH)* were used to normalize the target gene expression levels. The primer sequences are listed in Table S1.

Phloem transport assay

The phloem transport was assessed in the source leaves supporting the first raceme. A small area (~25 mm²) equidistant from the leaf margin and the midrib region was marked on the abaxial surface of fully expanded leaves. The cuticular layer was gently scrubbed with a scalpel, and a 10- μ L droplet of esculin solution (5 mg/mL; Alfa Aesar) was placed on the surface (De Moliner *et al.*, 2018; Knox *et al.*, 2018). The UV fluorescence indicating the esculin transport was documented at 0 and 10 min after esculin treatment using a Davinch-Gel imaging system MC-2000 (Davinch-K) under 306-nm UV light. The extent of esculin transport was quantified in terms of relative pixel intensity using ImageJ software.

Chlorophyll fluorescence measurements

The photosynthetic efficiency of the dark-adapted leaves from plants at 30 dpa was measured using an IMAGING-PAM chlorophyll fluorometer (MAXI Version; Walz). One measurement per plant was taken on young fully expanded leaves supporting the growth of the first raceme. Areas of interest with a diameter of 0.5 cm were randomly selected for recording data.

Measurement of leaf CO₂ assimilation rate

The instantaneous values of net CO₂ assimilation rate ($\mu\text{mol s}^{-1} \text{m}^{-2}$) in the source leaf were determined with an LI-6400 infrared gas analyzer (LI-COR). One measurement per plant was taken on young fully expanded leaves supporting the growth of the first raceme. Five to six different plants were used. The conditions in the measuring chamber were controlled at a flow rate of 500 mol s^{-1} , a saturating PAR of $1200 \mu\text{mol s}^{-1} \text{m}^{-2}$, $400 \mu\text{mol mol}^{-1} \text{CO}_2$, and $24 \text{ }^\circ\text{C}$ leaf temperature.

Plant phenotyping

The lengths and diameters of the peduncle and stem were manually quantified when at least half of the flowers were open in the inflorescences. The sizes (diameter) and weights of fruits were measured at the red ripe state. We used the first raceme from the bottom for measuring peduncle length. The diameters were measured with an electronic digital caliper (Mitutoyo). The peduncle lengths were evaluated using 30- and 60-cm standard rulers. The fresh weight of the fruits was recorded using a digital scale (CAS). The number of leaves, flowers, and fruits were counted in different genotypes of the same developmental age. The numbers of individuals quantified are indicated in the respective figures.

Acknowledgements

This work was supported by a grant from the New Breeding Technologies Development Program (project no. PJ016538), Rural Development Administration, Republic of Korea and the National Research Foundation of Korea (NRF) grant funded by the Korea government (MIST) (2020R1A2C3012750).

Conflict of interest

The authors declare that they have no conflict of interest.

Author contributions

Hoyoung Nam and Ildoo Hwang conceived and supervised this study; Hoyoung Nam, Aarti Gupta, and Ildoo Hwang designed the experiments; Hoyoung Nam, Heejae Nam, Hyun Seob Cho, Chanyoung Park, Soyoun Park, and Soon Ju Park performed the experiments and the data analysis; Hoyoung Nam, Aarti Gupta, Seungchul Lee and Ildoo Hwang wrote the original draft; and all authors reviewed and edited the manuscript.

References

- Ashikari, M., Sakakibara, H., Lin, S., Yamamoto, T., Takashi, T., Nishimura, A., Angeles, E.R. *et al.* (2005) Cytokinin oxidase regulates rice grain production. *Science*, **309**, 741–745.
- Bailey-serres, J., Parker, J.E., Ainsworth, E.A., Oldroyd, G.E.D. and Schroeder, J.I. (2019) Genetic strategies for improving crop yields. *Nature*, **575**, 109–118.
- Betti, M., Bauwe, H., Busch, F.A., Fernie, A.R., Keech, O., Levey, M., Ort, D.R. *et al.* (2016) Manipulating photorespiration to increase plant productivity: Recent advances and perspectives for crop improvement. *J. Exp. Bot.* **67**, 2977–2988.
- Cho, H., Cho, H.S., Nam, H., Jo, H., Yoon, J., Park, C., Dang, T.V.T. *et al.* (2018) Translational control of phloem development by RNA G-quadruplex–JULGI determines plant sink strength. *Nat. Plants*, **4**, 376–390.
- Cho, H., Dang, T.V.T. and Hwang, I. (2017) Emergence of plant vascular system: Roles of hormonal and non-hormonal regulatory networks. *Curr. Opin. Plant Biol.* **35**, 91–97.
- Cormier, F., Foulkes, J., Hirel, B., Gouache, D., Moënne-Loccoz, Y. and Le Gouis, J. (2016) Breeding for increased nitrogen-use efficiency: A review for wheat (*T. aestivum* L.). *Plant Breed.* **135**, 255–278.
- D'Aoust, M.-A., Yelle, S. and Nguyen-Quoc, B. (1999) Antisense inhibition of tomato fruit sucrose synthase decreases fruit setting and the sucrose unloading capacity of young fruit. *Plant Cell*, **11**, 2407–2418.
- Damari-Weissler, H., Rachamilevitch, S., Aloni, R., German, M.A., Cohen, S., Zwieniecki, M.A., Holbrook, N.M. *et al.* (2009) LeFRK2 is required for phloem and xylem differentiation and the transport of both sugar and water. *Planta*, **230**, 795–805.
- Dasgupta, K., Khadilkar, A.S., Sulpice, R., Pant, B., Scheible, W.R., Fisahn, J., Sitt, M. *et al.* (2014) Expression of sucrose transporter cDNAs specifically in companion cells enhances phloem loading and long-distance transport of sucrose but leads to an inhibition of growth and the perception of a phosphate limitation. *Plant Physiol.* **165**, 715–731.
- De Moliner, F., Knox, K., Reinders, A., Ward, J.M., McLaughlin, P.J., Oparka, K. and Vendrell, M. (2018) Probing binding specificity of the sucrose transporter AtSUC2 with fluorescent coumarin glucosides. *J. Exp. Bot.* **69**, 2473–2482.
- Ehrlich, P.R. and Harte, J. (2015) Opinion: To feed the world in 2050 will require a global revolution. *Proc. Natl. Acad. Sci. U. S. A.* **112**, 14743–14744.
- Gifford, R.M., Thorne, J.H., Hitz, W.D. and Giaquinta, R.T. (1984) Crop productivity and photoassimilate partitioning. *Science*, **225**, 801–808.
- Hackel, A., Schauer, N., Carrari, F., Fernie, A.R., Grimm, B. and Kühn, C. (2006) Sucrose transporter LeSUT1 and LeSUT2 inhibition affects tomato fruit development in different ways. *Plant J.* **45**, 180–192.
- Heo, J., Roszak, P., Furuta, K.M. and Helariutta, Y. (2014) Phloem development: Current knowledge and future perspectives. *Am. J. Bot.* **101**, 1393–1402.
- Ho, L.H., Klemens, P.A.W., Neuhaus, H.E., Ko, H.Y., Hsieh, S.Y. and Guo, W.J. (2019) SISWEET1a is involved in glucose import to young leaves in tomato plants. *J. Exp. Bot.* **70**, 3241–3254.
- Hwang, I. and Sheen, J. (2001) Two-component circuitry in *Arabidopsis* cytokinin signal transduction. *Nature*, **413**, 383–389.
- Kallarackal, J. and Milburn, J.A. (1984) Specific mass transfer and sink-controlled phloem translocation in Castor Bean. *Aust. J. Plant. Physiol.* **11**, 483–490.
- Kang, B.C., Wook, J.W., Kim, S.T., Bae, S.J., Choi, M., Kim, J.S. and Kim, S.G. (2019) Guidelines for C to T base editing in plants: Base-editing window, guide RNA length, and efficient promoter. *Plant Biotechnol. Rep.* **13**, 533–541.
- Kikin, O., D'Antonio, L. and Bagga, P.S. (2006) QGRS Mapper: A web-based server for predicting G-quadruplexes in nucleotide sequences. *Nucleic Acids Res.* **34**, 676–682.
- Knoblauch, M., Vendrell, M., de Leau, E., Paterlini, A., Knox, K., Ross-Elliott, T., Reinders, A. *et al.* (2015) Multispectral phloem-mobile probes: properties and applications. *Plant Physiol.* **167**, 1211–1220.
- Knox, K., Paterlini, A., Thomson, S. and Oparka, K. (2018) The coumarin glucoside, esculin, reveals rapid changes in phloem-transport velocity in response to environmental cues. *Plant Physiol.* **178**, 795–807.
- Kwon, C.T., Heo, J., Lemmon, Z.H., Capua, Y., Hutton, S.F., Van Eck, J., Park, S.J. *et al.* (2020) Rapid customization of solanaceae fruit crops for urban agriculture. *Nat. Biotechnol.* **38**, 182–188.
- Liu, H., Ding, Y., Zhou, Y., Jin, W., Xie, K. and Chen, L.L. (2017) CRISPR-P 2.0: An improved CRISPR-Cas9 tool for genome editing in plants. *Mol. Plant.* **10**, 530–532.
- Long, S.P., Marshall-Colon, A. and Zhu, X.G. (2015) Meeting the global food demand of the future by engineering crop photosynthesis and yield potential. *Cell*, **161**, 56–66.
- López-Salmerón, V., Cho, H., Tonn, N. and Greb, T. (2019) The phloem as a mediator of plant growth plasticity. *Curr. Biol.* **29**, R173–R181.
- Lu, M., Snyder, R., Grant, J. and Tegeder, M. (2020) Manipulation of sucrose phloem and embryo loading affects pea leaf metabolism, carbon and nitrogen partitioning to sinks as well as seed storage pools. *Plant J.* **101**, 217–236.
- Lucas, W.J., Groover, A., Lichtenberger, R., Furuta, K., Yadav, S.R., Helariutta, Y., He, X.-Q. *et al.* (2013) The plant vascular system: Evolution, Development and Functions. *J. Integr. Plant Biol.* **55**, 294–388.

- Micallef, B.J., Haskins, K.A., Vanderveer, P.J., Roh, K., Shewmaker, C.K. and Sharkey, T.D. (1995) Altered photosynthesis, flowering, and fruiting in transgenic tomato plants that have an increased capacity for sucrose synthesis. *Planta*, **2**, 327–334.
- Millar, A.A. and Gubler, F. (2005) The Arabidopsis GAMYB-Like genes, MYB33 and MYB65, are MicroRNA-regulated genes that redundantly facilitate anther development. *Plant Cell*, **17**, 705–721.
- Mills, G., Sharps, K., Simpson, D., Pleijel, H., Frei, M., Burkey, K., Emberson, L. et al. (2018) Closing the global ozone yield gap: Quantification and cobenefits for multistress tolerance. *Glob. Chang. Biol.* **24**, 4869–4893.
- Mishra, R., Joshi, R.K. and Zhao, K. (2020) Base editing in crops: Current advances, limitations and future implications. *Plant Biotechnol. J.* **18**, 20–31.
- Murchie, E.H. and Niyogi, K.K. (2011) Manipulation of photoprotection to improve plant photosynthesis. *Plant Physiol.* **155**, 86–92.
- Murray, M.G. and Thompson, W.F. (1980) Rapid isolation of high molecular weight plant DNA. *Nucleic Acids Res.* **8**, 4321–4326.
- Nguyen, C.D., Mansfield, R.E., Leung, W., Vaz, P.M., Loughlin, F.E., Grant, R.P. and MacKay, J.P. (2011) Characterization of a family of RanBP2-Type zinc fingers that can recognize single-stranded RNA. *J. Mol. Biol.* **407**, 273–283.
- Osorio, S., Ruan, Y.L. and Fernie, A.R. (2014) An update on source-to-sink carbon partitioning in tomato. *Front. Plant Sci.* **5**, 1–11.
- Patrick, J.W. (2013) Does Don Fisher's high-pressure manifold model account for phloem transport and resource partitioning? *Front. Plant Sci.* **4**, 1–17.
- Peng, J., Richards, D.E., Hartley, N.M., Murphy, G.P., Devos, K.M., Flintham, J.E., Beales, J. et al. (1999) "Green revolution" genes encode mutant gibberellin response modulators. *Nature*, **400**, 256–261.
- Price, G.D., Badger, M.R., Woodger, F.J. and Long, B.M. (2008) Advances in understanding the cyanobacterial CO₂-concentrating-mechanism (CCM): Functional components, Ci transporters, diversity, genetic regulation and prospects for engineering into plants. *J. Exp. Bot.* **59**, 1441–1461.
- Ray, D.K., Mueller, N.D., West, P.C. and Foley, J.A. (2013) Yield trends are insufficient to double global crop production by 2050. *PLoS One*, **8**, e66428.
- Regmi, K.C., Yogendra, K., Farias, J.G., Li, L., Kandel, R., Yadav, U.P., Sha, S. et al. (2020) Improved yield and photosynthate partitioning in AVP1 expressing wheat (*Triticum aestivum* L.) plants. *Front. Plant Sci.* **11**, 1–16.
- Reuscher, S., Akiyama, M., Yasuda, T., Makino, H., Aoki, K., Shibata, D. and Shiratake, K. (2014) The sugar transporter inventory of tomato: Genome-wide identification and expression analysis. *Plant Cell Physiol.* **55**, 1123–1141.
- Rodriguez-Leal, D., Lemmon, Z.H., Man, J., Bartlett, M.E. and Lippman, Z.B. (2017) Engineering quantitative trait variation for crop improvement by genome editing. *Cell*, **171**, 1–11.
- Rottmann, T.M., Fritz, C., Lauter, A., Schneider, S., Fischer, C., Danzberger, N., Dietrich, P. et al. (2018) Protoplast-esculin assay as a new method to assay plant sucrose transporters: Characterization of AtSUC6 and AtSUC7 sucrose uptake activity in arabidopsis Col-0 ecotype. *Front. Plant Sci.* **9**, 1–22.
- Ru, L., He, Y., Zhu, Z., Patrick, J.W. and Ruan, Y.L. (2020) Integrating sugar metabolism with transport: Elevation of endogenous cell wall invertase activity up-regulates *SIHT2* and *SISWEET12c* expression for early fruit development in tomato. *Front. Genet.* **11**. <https://doi.org/10.3389/fgene.2020.592596>
- Ruan, Y. (2014) Sucrose metabolism: gateway to diverse carbon use and sugar signaling. *Annu. Rev. Plant Biol.* **65**, 33–67.
- Ruan, Y.L., Patrick, J.W., Bouzayen, M., Osorio, S. and Fernie, A.R. (2012) Molecular regulation of seed and fruit set. *Trends Plant Sci.* **17**, 656–665.
- Sasaki, A., Ashikari, M., Ueguchi-Tanaka, M., Itoh, H., Nishimura, A., Swapan, D., Ishiyama, K. et al. (2002) A mutant gibberellin-synthesis gene in rice. *Nature*. **416**, 701–702.
- Schimpl, S., Fauser, F. and Puchta, H. (2014) The CRISPR/Cas system can be used as nuclease for *in planta* gene targeting and as paired nickases for directed mutagenesis in Arabidopsis resulting in heritable progeny. *Plant J.* **80**, 1139–1150.
- Shammai, A., Petreikov, M., Yeselson, Y., Faigenboim, A., Moy-Komemi, M., Cohen, S., Cohen, D. et al. (2018) Natural genetic variation for expression of a SWEET transporter among wild species of *Solanum lycopersicum* (tomato) determines the hexose composition of ripening tomato fruit. *Plant J.* **96**, 343–357.
- Shimatani, Z., Kashojiya, S., Takayama, M., Terada, R., Arazoe, T., Ishii, H., Teramura, H. et al. (2017) Targeted base editing in rice and tomato using a CRISPR-Cas9 cytidine deaminase fusion. *Nat. Biotechnol.* **35**, 441–443.
- Smith, M.R., Rao, I.M. and Merchant, A. (2018) Source-sink relationships in crop plants and their influence on yield development and nutritional quality. *Front. Plant Sci.* **871**, 1–10.
- Sun, H.J., Uchii, S., Watanabe, S. and Ezura, H. (2006) A highly efficient transformation protocol for Micro-Tom, a model cultivar for tomato functional genomics. *Plant Cell Physiol.* **47**, 426–431.
- Taiz, L. (2013) Agriculture, plant physiology, and human population growth: past, present, and future. *Theor. Exp. Plant Physiol.* **25**, 167–181.
- Wang, L., Lu, Q., Wen, X. and Lu, C. (2015) Enhanced sucrose loading improves rice yield by increasing grain size. *Plant Physiol.* **169**, 2848–2862.
- Weichert, H., Högy, P., Mora-Ramirez, I., Fuchs, J., Eggert, K., Koehler, P., Weschke, W. et al. (2017) Grain yield and quality responses of wheat expressing a barley sucrose transporter to combined climate change factors. *J. Exp. Bot.* **68**, 5511–5525.
- White, A.C., Rogers, A., Rees, M. and Osborne, C.P. (2016) How can we make plants grow faster? A source-sink perspective on growth rate. *J. Exp. Bot.* **67**, 31–45.
- Yadav, U.P., Ayre, B.G. and Bush, D.R. (2015) Transgenic approaches to altering carbon and nitrogen partitioning in whole plants: Assessing the potential to improve crop yields and nutritional quality. *Front. Plant Sci.* **6**, 1–13.
- Yu, S.M., Lo, S.F. and Ho, T.H.D. (2015) Source-sink communication: Regulated by hormone, nutrient, and stress cross-signaling. *Trends Plant Sci.* **20**, 844–857.
- Zhang, C. and Turgeon, R. (2018) Mechanisms of phloem loading. *Curr. Opin. Plant Biol.* **43**, 71–75.
- Zhang, L., Garneau, M.G., Majumdar, R., Grant, J. and Tegeder, M. (2015) Improvement of pea biomass and seed productivity by simultaneous increase of phloem and embryo loading with amino acids. *Plant J.* **81**, 134–146.
- Zhu, L., Li, B., Wu, L., Li, H., Wang, Z., Wei, X., Ma, B. et al. (2021) MdERDL6-mediated glucose efflux to the cytosol promotes sugar accumulation in the vacuole through up-regulating TSTs in apple and tomato. *Proc. Natl. Acad. Sci. U. S. A.* **118**, 1–12.

Supporting information

Additional supporting information may be found online in the Supporting Information section at the end of the article.

Figure S1 Subcellular localization of the *SIJUL*-GFP and *SIJUL*^{R20/81/151A}-GFP fusions expressed in Arabidopsis protoplasts.

Figure S2 Expression pattern of *SIJUL* in different organs.

Figure S3 Characterization of *SIJUL* knockdown by VIGS in source and sink tissues.

Figure S4 Expression profile of cambium and xylem marker genes.

Figure S5 Molecular characterization of stable *sljul*-Cas9 knock-out plants.

Figure S6 Molecular and functional characterization of *sljul-d4*-Cas9 plants.

Figure S7 Characterization of phloem transport capacity in *TRV-SIJUL* knockdown plants.

Figure S8 Dimensions of sieve tubes in *TRV-SIJUL* knockdown plants.

Figure S9 Fruit sugar contents in *TRV-SIJUL* and *TRV-GFP* plants.

Figure S10 Characterization of resource allocation and the trade-off in *TRV-SIJUL* knockdown plants.

Figure S11 Schematic diagram showing a proposed model demonstrating the correlation among phloem development, photoassimilate distribution, and productivity.

Table S1 List of primers used in the study.